MODEL OF CONDUCTIVITY FOR PEROVSKITES BASED ON THE SCALING PROPERTY OF GRAIN BOUNDARY

Phung Quoc Thanh, Hoang Nam Nhat, Bach Thanh Cong

Department of Physics, College of Sciences - VNU

Abstract. We present the percolation-theory model for explanation of conductivity of perovskites based on the scaling property of grain boundary formation. Assuming a two-layer simple effective medium model, composed of the grain itself as a first layer and the boundary as a second layer, it was modeled that the net resistivity r of the medium depends on the average grain size L, boundary thickness L' and boundary fractal dimension D. The obtained formula was tested specifically for the perovskite system $Ca_{0.85}Pr_{0.15}Mn_{1-x}Ru_xO_3$ (x=0.00, 0.03, 0.05 and 0.07) whose structures and electric properties were reported earlier by these authors [VNU J. of Sci., XX, No.3 AP, 2004, p. 130-132]. The determination of fractal dimension was based on the standard length-area technique and was carried out using SEM images which were photographed at three magnification scales 2, 5 and 10μm. This dimension showed good correspondence to the small polaron hoping energy in high temperature region and gave very good fits to experimental data for T$< T_N$.

Perovskite; Structure; Fractal; Grain; Boundary; Conductivity
PACS: 47.53.+n Fractals - 61.72.Mn Grains - 91.60.Ed Crystal structure and defects

1. Introduction

The application of the fractal techniques to study the conduction mechanism in the perovskite superconductors [1-3] is not new, but for the manganate perovskites there is a lack of studies dealing directly with the grain boundary conductivity. We know only one work from Dobrescu et al. reporting the fractal dimension determination for $La_{1-x}Sr_xCoO_3$ [4]. Although many studies showed the essential effects of grain boundary on the macroscopic resistivity of perovskite [5], up-to-date there is still absent the knowledge about the boundary geometry. For the perovskites, one may adopt the fractal model and the method for determination of dimension from the studies for metal oxides, such as for the iron quartizites [6]. Here the measurement of the voltage drop distribution across the square matrix settled by the Werner arrays was performed. The apparent resistivity was expected to depend on the electrode separation l according to:

$$\rho \propto l^D \tag{1}$$

with D is the critical exponent related to the fractal dimension of the mozaic boundary system underlying the measured matrix. It is also known that near the threshold concentration x_c, the effective resistivity of the percolation system behaves as:

$$\rho \propto (x - x_c)^{D'} \tag{2}$$

with D' is another critical exponent. The above relations, however, do not include the term for the temperature dependence. The common approach for $T < T_c$ was to consider (see Rao and Raychaudhury in [5]):

$$\rho = \rho_0 + \rho_1 T^n \tag{3}$$

with the exponent $n \approx 2.5$ and the ratio $\rho_1/\rho_0 \approx 10^{-6}$. For $T > T_c$, the usual attitude was to suggest either the small polaron hoping or the bandgap conduction model. Both rely on the exponential development of ρ according to T: Small polaron:

$$\rho \propto T \exp(W_p/k_B T) \tag{4}$$

Bandgap:

$$\rho \propto \exp(E_a/k_B T), \tag{5}$$

where the W_p stands for the polaron hoping energy and E_a for the activation energy. Some authors reported the variable hoping model with $\rho \propto \exp[(T_0/T)^{1/4}]$ to be suitable for the manganate perovskites, but we found this relation to be fitted worse in the tested samples (see Section 3).

2. Boundary resistivity from fractal viewpoint

We now adopt the two-layer simple effective medium model for the resistivity as has been used in Gupta et al. [7]. Consider two homogeneous media, the grain itself with size L and resistivity ρ_G and the boundary with thickness L' and resistivity ρ_B. The net resistivity is:

$$\rho = \rho_G + (L'/L)\rho_B \tag{6}$$

Since the grains consist of the disordered single crystal pieces, it is evident to suggest that above T_c the intra-grain resistivity ρ_G evolutes according to (4) or (5). This resistivity may be influenced by the intra-grain single crystal boundary but it is not expected to depend on the inter-grain boundary. The boundary resistivity ρ_B may be given, according to (1) - (3), as:

$$\begin{aligned} \rho_B &= (\rho_0 + \rho_1 T_n)(x - x_c)^{D'} l^D \\ &= (\rho_0 + \rho_1 T^n)(x - x_c)^{D'} (kL)^D = f\rho_0 + f\rho_1 T^n \end{aligned} \tag{7}$$

with $f = (k^D L' L^{D-1})(x - x_c)^{D'}$. For each percolation system, the constant factor f is determined by the system composition and geometry. By fitting (7) to the experiment data, the exponent n and ρ_0, ρ_1 could be found. The ρ_0 refers to the temperature-independent part of the boundary resistivity whereas the ρ_1 to the temperature-dependent part. The problem was not, however, the determination of n, D or D' but their physical foundation. The procedures that were involved to estimate D, e.g. in [6], do not strictly relate D to

the boundary resistivity. As the measured resistivity heavily depends on the method and the apparature settlement, the obtained D only refers to the applied apparent resistivity. At this moment there is no way to prove that D really corresponds to the true boundary resistivity. For the purpose of the first approximation, we must adopt the asumption that the D, estimated by the procedure described below, closely conforms to the D obtained by measuring the apparent resistivity ρ.

To estimate D we used the classical length-area relation, e.g. described in [8]. For each SEM magnification (each yardstick) G, the ratio $l_G = L_S/L_A$ of the linear extents L_S, determined on the basis of the grain domain perimeter $G - length$ (in unit of image size) and L_A, determined on the basis of the grain domain area $G - area$ (in unit of image area), is a constant:

$$l_G = L_S/L_A = (G - Length)^{1/D}/(G - area)^{1/2} \approx constant \tag{8}$$

with D be interpreted as the fractal dimension of the grain boundary. Reasonably, for the two different magnifications G' and G the ratio:

$$l_{G'}/l_G = (G'/G)^{1/D-1} \tag{9}$$

Evidently, the log-log plot from the relations (8)-(9) reveals the fractal dimension D.

3. Test samples: $Ca_{0.85}Pr_{0.15}Mn_{1-x}Ru_xO_3$

Let us review the structure determination of the test samples that has been reported in [9]. The $Ca_{0.85}Pr_{0.15}Mn_{1-x}Ru_xO_3$ (x=0.00, 0.03, 0.05 and 0.07) samples were prepared using the standard ceramic technique. All samples exhibit the orthorhombic space group $Pbnm$ with the unit cell volumes slightly increased as Ru content grows. The average single crystal size was: 24.0, 24.5, 25.3 and 26.1nm for the growing x. The typology of surfaces was studied by SEM where images with different magnification (of order 2, 5 and 10μm) were taken at different surface positions. Fig.1 shows one image at 10-μm scale for $x = 0.03$, the rest was omitted for clarity. The determined average grain size was 3750, 1030, 2360 and 3300nm for x from 0.00 to 0.07 sequentially (which means approx. 156, 42, 93 and 126 single crystal pieces within each grain, respectively).

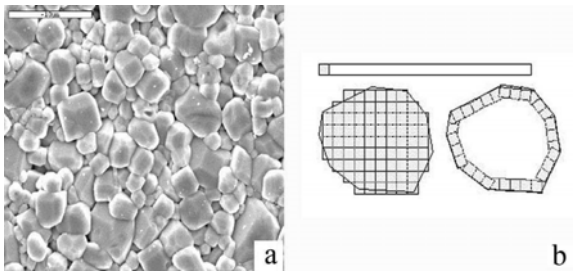

Fig.1. SEM image of surface for the sample x=0.03 at the 10μm scale (a). A sample segmentation into the squares for calculation of the fractal dimension (b).

We have re-measured the electric resistance by the standard four electrode technique in the temperature range from 10 to 350K for each 5K step. The results for the conductivity measurement is shown in Fig.2. These compounds showed the constant semiconductor character with quite low resistivity at the room temperature (of order $1 - 10\Omega cm$). The FC magnetization curves reported in [10] showed $T_N \approx 120K$. In the high temperature region, the fitted results against the small polaron model showed a little better linear correlation ($R^2 > 0.98$) compared to that of the band gap model ($R^2 > 0.96$). It is really difficult to distinguish between the two models in the limited temperature region.

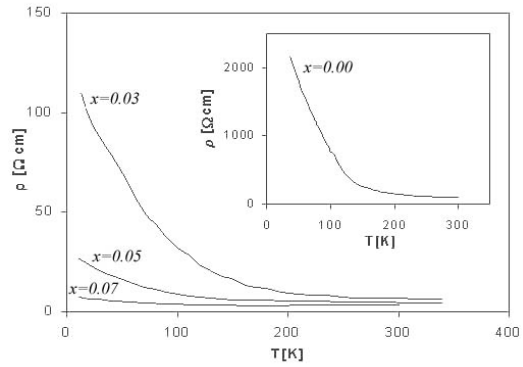

Fig.2. The development of resistivity from 10K to 350K for $x = 0.03 - 0.07$. The inset shows $x = 0.00$.

For the whole temperature range, both models showed the sharp declines from the linearity at the temperature near T_N, whereas the variable hoping model showed relatively good fit ($R^2 > 0.95$), both above and below T_N (Fig.3).

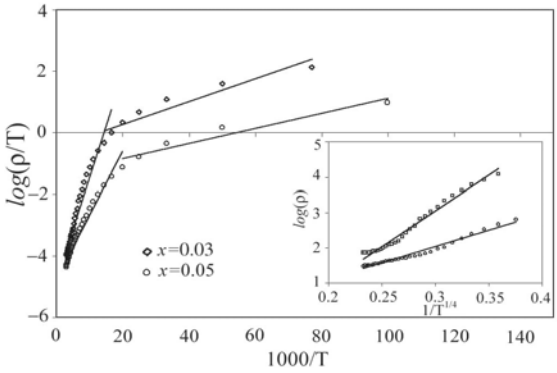

Fig.3. The fits for the small polaron hoping model for two cases $x = 0.03$ and 0.05 (other two cases are omitted for clarity) show the sharp declines from the linearity at the temperatures near T_N. The linear approximation in the high temperature region has $R^2 > 0.98$.The inset shows the fit due to the variable hoping model. Although the linearity was less, this fits the whole temperature range well.

In Fig.4 we show the differential curve $dln(\rho)/d(1/T)$ drawn together with the original $ln(\rho)$ vs. $1000/T$ curve for $x = 0.03$. As seen, the $ln(\rho)$ drops at the lower T. Since the $dln(\rho)/d(1/T)$ corresponds to the activation energy, its drop signifies the variation of this energy and for our case, this means the change in conduction mechanism. The estimation for W_P from the slopes of $log(\rho/T)$ vs. $1000/T$ yields 0.52, 0.43, 0.27 and 0.17eV for $x = 0.00 - 0.07$, in sequence.

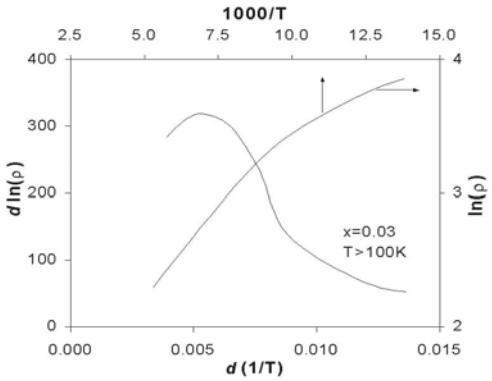

Fig.4. The differential curve $dln(\rho)/d(1/T)$ drawn against $1/T$ for $x = 0.03$ reveals the drop of the activation energy when the temperature decreases. This argues for the change in conduction mechanism away from the bandwidth-controlled conduction to the possible boundary-controlled percolative conduction.

To fit the data in the low temperature region we estimated the fractal dimension D, needed in relation (7), according to the following procedure. First, measure the total area of each SEM photograph, then divide this area into the smaller squares and use them to fill each grain area. The number of squares filled into one grain is just the $G - area$ and the number of squares that cross-over the grain or run over the grain boundary is just the linear extend $G - Length$. The log-log plot from these two quantities determines D (Fig.5).

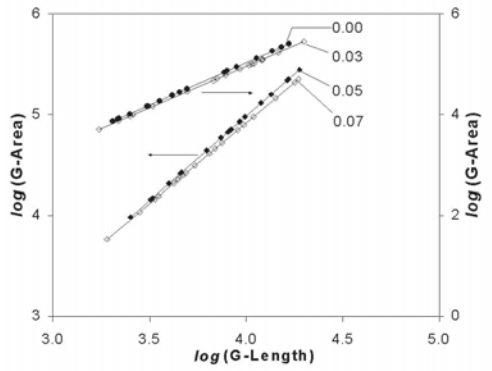

Fig.5. The $log(G - Area)$ vs. $log(G - Length)$ plot.

Table 1 summarizes the measurement details and results (D, f, L and L'). For the calculation of f, the percolation threshold concentration x_c was set to zero since all samples are above threshold; the concentration x was set equal to the Mn^{4+}/Mn^{3+} ratio estimated by the Rietveld refinement [9] (also see Rao and Raychaudhury in [5]) and D' was assumed equal to D. A larger grain size L tends to the smaller D. These D-s correspond well to the W_P, except for $x = 0.00$, as seen in Fig.7.

TABLE 1. The fractal analysis of boundary characteristics for $Ca_{0.85}Pr_{0.15}Mn_{1-x}Ru_xO_3$.

Sample x	No. of meas.	Square size [magn. scale]	L (±δ) [nm]	L' (δ in paren.) [nm]	D (±δ)	f [$\times 10^5$]	x
0.00	27	1/15-1/40	3750±15	3.2(1)	1.18±0.02	0.62	0.92
0.03	37	1/10-1/50	1030±17	1.5(2)	1.25±0.03	3.49	1.00
0.05	42	1/10-1/50	2360±14	2.3(7)	1.22±0.03	1.64	1.08
0.07	40	1/15-1/40	3300±10	2.9(2)	1.20±0.02	1.17	1.17

Fig.6 shows the fit results for two cases $x = 0.03$ and 0.05 (the inset). The dotted lines denote the fit according to the small polaron model (4) whereas the lines are according to (7). The least square figure of merit $R < 0.02$. The temperature at which the lines and the dotted lines cross over is 120K ($x = 0.03$) and 110K ($x = 0.05$). This temperature drops to 100K for $x = 0.07$. Compared to FC curves [10], these temperatures correspond to the Neel temperature T_N of the charge-ordering antiferromagnetic-to-paramagnetic phase transitions. Table 2 lists the power factor n, the constant ρ_0 and ρ_1 that were determined from the fits. The n grew linearly with W_P better than D with W_P (Fig.7).

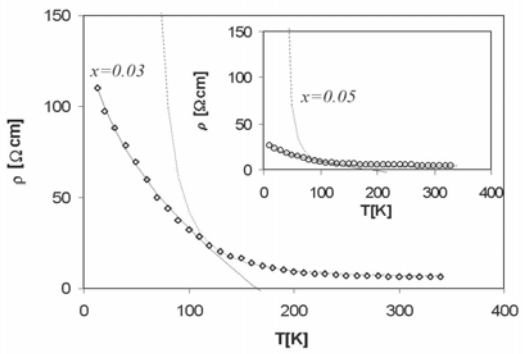

Fig.6. The fit examples for $x = 0.03$ and 0.05 (the inset) according to (4) (high T region) and (7) (low T region). The least square figure of merit $R < 0.02$. The cross points showed the estimated T_N for each case to be 120K ($x = 0.03$) and 110K ($x = 0.05$).

Recall the approximation for the boundary resistivity was $6 \times 10^2 \Omega cm$ [5,7] (confirmed to the very low boundary conductivity of 10^{-5} in unit of $e^2/\hbar$). Our model estimated the pure boundary resistivity to be ρ_0 of order $50 \times 10^{-5} \Omega cm$ (Table 2), which suggests the conductivity of order 10 $e^2/\hbar$. Since the $(e^2/\hbar)$ corresponds to the minimal

Mott conductivity, the value of 10 is a much better estimation for the boundary conductivity than the one 10^{-5} reported earlier.

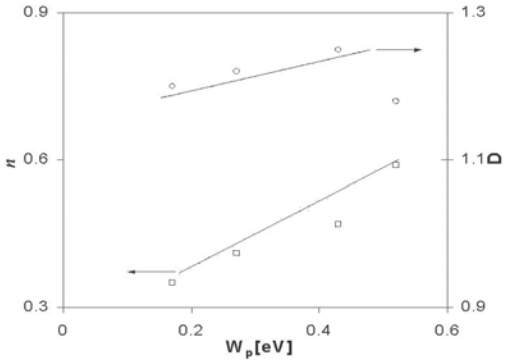

Fig.7. The relations between D, n and W_p show almost linearity between n and W_p, whereas this linearity holds for D only if excluding the case $x = 0.00$.

TABLE 2. The fitting results for the power factor n, the constants ρ_0 and ρ_1

Sample x	n	ρ_0 [$\times 10^{-5}\,\Omega$cm]	ρ_1 [$\times 10^{-5}\Omega$cm]
0.00	0.59	6099.0	−321.0
0.03	0.47	45.4	−4.2
0.05	0.41	23.5	−2.7
0.07	0.35	8.65	−1.1

Conclusions

This work is the first of its kind to apply the fractal analysis to study the boundary conduction in perovskites. The use of the fractal technique in perovskites faces several limitations due to the small size of the samples that usually do not allow the manufacture of the Werner array electrode matrix. We showed that by using the SEM images, the boundary fractal dimension and the related boundary geometric properties, such as the average size and thickness, might be well estimated, and that the estimated values successfully described the temperature behaviours of the resistivity for the tested samples. Furthermore, the fractal dimension showed very good correspondence to the small polaron hoping energy in the high temperature region. They also developed linearly with the critical exponents n in the low temperature region; this fact argues for the fractal nature of n, but the confirmation needs further investigation. In contrast to the fractal dimension determined on the basis of the voltage drop distribution across the Werner array matrix, the dimension measured using the SEM images really belongs to the boundary system but it lacks to bind to the apparent resistivity by its nature. At this stage, their incorporation into the relation (7) was purely a model. To confirm this model, one needs to arrange the

Werner array matrix on the samples, that is to build at least 40×40 electrodes onto a surface area approx. $1cm^2$. We leave this experiment for the future consideration.

References

1. Daolun Chen, Dexing Pang, Zhongjin Yang, Sa Kong, Litian Wang, Ke Yang and Guiwen Qiao, The relationship between superconductivity and microstructure through the fractal dimensions in Y-Ba-Cu-O compounds, *J. Phys. C: Solid State Phys.* **21**(1988), L271-L276.
2. J.C. Phillips, Superconducting and Related Oxides: Physics and Nanoengineering III, *SPIE Proc.*, (Ed. D. Pavuna and I Bozovic), **3481**(1998) p. 87.
3. J. C. Phillips, Fractal Nature and Scaling Exponents of Non-Drude Currents in Non-Fermi Liquids, *arXiv:cond-mat/0104095.*
4. G. Dobrescu, D. Berger, F. Papa, N. I. Ionescu, M. Rusu, Fractal analysis of micrographs and adsorption isotherms of La1-xSrxCoO3 samples, *Journal of Optoelectronics and Advanced Materials,* Vol.5, **No.5**(2003).
5. C.N.Rao and B. Raveau, *Collossal Magnetoresistance, Charge Ordering and Related Properties of Manganese Oxides*, World Scientific Publishing Co., Singapore 1998.
6. S.S.Krylov, V.F.Lubchich, The Apparent Resistivity Scaling and Fractal Structure of an Iron Formation, Izvestia, *Physics of the Solid Earth*, Vol.38 **No.12**(2002), pp. 1006-1012. Translated from Fizika Zemli, No 12, 2002, pp 14-21.
7. A. Gupta, G. Q. Gong, Gang Xiao, P. R. Duncombe, P. Lecoeur, P. Trouilloud,Y.Y. Wang, V. P. Dravis and J. Z. Sun, *Phys. Rev. B54*(1996) R15629.
8. B.B. Mandelbrot, *The Fractal Geometry of Nature*, W.H. Freeman and Co., New York, NY 1983, (Chapter IV, 12 Length-Area-Volume Relations), p. 110-111.
9. P. Q. Thanh, H.N. Nhat and B.T. Cong, *VNU J. of Science,* T.XX, **No.3 AP,**(2004), p. 130-132.
10. P. Q. Thanh, B.T. Cong, N.N. Dinh, *Private communication.*